Assessment of implicit and explicit models for different photovoltaic modules technologies

N. Boutana [a], A. Mellit [a, b, *], V. Lughi [c], A. Massi Pavan [c, d]

[a] Renewable Energy Laboratory, Faculty of Sciences and Technology, Electronics Department, Jijel University, Ouled-Aissa, P.O. Box .98, Jijel, 18000, Algeria
[b] The Abdus Salam International Centre for Theoretical Physics (ICTP), Starada Costiera, 11, 34151, Trieste, Italy
[c] Department of Engineering and Architecture, University of Trieste, Via A. Valerio, 6/A, 34127, Trieste, Italy
[d] The School of Electrical and Electronic Engineering, The University of Manchester, Manchester, UK

ARTICLE INFO

Accepted 14 January 2017

Keywords:
Photovoltaic module
Modelling and simulation
Implicit model
Explicit model

ABSTRACT

Effective use of photovoltaic (PV) modules requires reliable models for a number of applications, such as monitoring the performance of PV systems, estimating the produced power and plant design, etc. Development of accurate and simple models for different PV technologies remains a big challenge. In this paper, a comparative study of seven implicit and explicit models, published in the literature, is presented. The predicted current-voltage characteristics of the main commercial PV module technologies (multi-crystalline Silicon, Copper Indium Gallium Selenide, and Cadmium Telluride), have been compared both with the ones from the datasheet and with the ones obtained experimentally. Moreover, the investigated models have also been evaluated in terms of accuracy, required parameters, generalisation capability and complexity.

1. Introduction

Photovoltaics (PV) is expanding very rapidly: the total installed PV capacity at the end of 2015 amounted globally to 200 GW [1] becoming in some countries (such as Italy or Germany) a key contributor to power generation. This expansion is the result of effective supporting policies as well as of drastic cost reductions which are in part a feedback effect determined by the economy of scale that follows market expansion, in part the result of technological and industrial improvements. The efficiency of PV modules has grown considerably. The highest reported efficiency of the most common used PV technologies is 23.8% for large crystalline silicon-based modules (m-Si), 12.3% for tandem amorphous Silicon (a-Si), and 18.6% and 17.5% for Cadmium Telluride (CdTe) and Copper Indium Gallium Selenide (CIGS) thin film-based modules [2], respectively, while the actual efficiency of the corresponding commercial products is normally 2–4% points lower (absolute); meanwhile the production cost of PV modules decreased dramatically, and the combined effect is a significant reduction of the cost-per-kWh – the key figure of merit for evaluating energy sources.

A key parameter for evaluating the cost-per-kWh (specifically, the Levelized Cost Of Energy – LCOE) is the energy yield. Models for cells or modules are increasingly being used by researchers, plant designers operation and maintenance personnel, electric grid operators, for prediction of the energy yield of PV systems [3]. As the economic figures of a PV plant are quite sensitive to the energy yield, the accuracy of such models is the key for sound decisions and policy making regarding PV installations and development.

Some studies have been conducted on the performance parameters of PV modules under different climatic conditions. For example, in Ref. [4] the authors performed a comparative analysis of the efficiency of different module technologies under the climatic conditions of Southern Spain. An implicit correlation for the operating temperature of crystalline PV modules under real use conditions has been proposed in Ref. [5]. A thermal model is proposed in Ref. [6], that incorporates atmospheric conditions, the effects of PV module material composition and mounting structure, during periods of rapidly changing conditions. In Ref. [7] the authors assessed five different models for predicting the temperature of the solar PV module, the output power and efficiency for sunny days with different solar radiation intensities and ambient temperatures. An analytical modelling approach for estimating the outdoor performance of thin film PV modules in inland sites with

* Corresponding author. Renewable energy laboratory, Faculty of Sciences and technology, Electronics Department, Jijel University, Ouled-Aissa, P.O. Box .98, Jijel, 18000, Algeria.
E-mail addresses: adel_mellit@univ-jijel.dz, amellit@ictp.it (A. Mellit).

Nomenclature

μ_{Isc}	current/temperature coefficient
μ_{Voc}	voltage/temperature coefficient
γ	shape parameter 1
a_1	ideality factor of diode1
a_2	ideality factor of diode2
$FF_{T,G}$	fill factor at a temperature T and irradiance G
$FF_{o,G}$	fill factor at a temperature 25 °C and irradiance G
G	irradiance (W/m^2)
I	output current (A)
I_{mp}	current at the maximum power point (A)
I_o	diode reverse saturation current (A)
I_{ph}	photocurrent (A)
I_{sc}	short circuit current (A)
k	Boltzmann constant (1.38006e-23 J/K)
m	exponential factor
N_s	number of cells in series
n	shape parameter2
P_{mp}	maximum power point (W)
v_{mp}	normalized maximum power voltage
q	electron charge (1.60218e-19 C)
$r_{sT,G}$	normalized series resistance at a temperature T and irradiance G
R_s	series resistance (Ω)
R_{sh}	shunt resistance (Ω)
T	cell temperature (°C)
V	output voltage (V)
V_{mp}	voltage at the maximum power point (V)
V_{oc}	open circuit voltage (V)
V_t	thermal voltage (V)

sunny climates is presented in Ref. [8]. In addition, several models for determining the current-voltage (I-V) and power-voltage (P-V) characteristics of PV cells and modules are currently available in the literature. Many of these models come from the standard single- and two-diode models [9–12], and can be classified as implicit or explicit [3,13].

Implicit models [14–18] are mainly based on nonlinear equations which require iterative calculations and a non-negligible computational effort to estimate the parameters of the solar cell/module, which are not available from manufacturers' datasheets, such as the photocurrent, the series and shunt resistances, the diode ideality factor, the diode reverse saturation current, and the band-gap energy of the semiconductor. In fact, manufacturers typically provide only a limited data set for PV modules, such as the open-circuit voltage (V_{oc}), the short-circuit current (I_{sc}), the maximum power current (I_{mp}), and voltage (V_{mp}). Moreover, these data are only available at Standard Test Conditions (STC). For such conditions, PV modules produce a high power output, but they are rarely encountered in actual operation. A number of algorithms based on evolutionary approaches have been developed to estimate the parameters, for example particle swarm optimization [19], differential evolution [20], pattern search [21], genetic algorithms (GAs) [22] and artificial neural networks (ANNs) [23], however, the calculation process is complicated.

Explicit models [13,24–30] are mainly based on simple analytical expressions, which enable designers and engineers to determine the key parameters of a solar cell or module without using iterative numerical calculations. The use of explicit models is also an advantage for users as computer-aided computations are more easily implemented.

The main objective of this work is to make a comparative study of seven implicit [14,15,18] and explicit [13,24,26,28] models available in the literature. The models have been assessed by using manufacturers and experimental data (I-V characteristics) for a number of PV module technologies (m-Si, CIGS and CdTe). The focus of this paper is to verify the effectiveness of these models for different photovoltaic technologies (owning both to the first and the second generation), and different working conditions (of cell temperature and solar irradiance).

2. PV models

Numerous solar cell models are available in the literature. The models investigated in this work are reported in Table 1. The models have been selected among well-known models, based on their simplicity, required parameters and easiness of implementation.

2.1. Implicit models

Modelling of PV solar cells requires electrical parameters which are dependent on the device architecture and the materials.

2.1.1. Sera et al. model

The single diode model, shown in Fig. 1, emulates the PV characteristics. The current-voltage (I-V) relationship of PV cell is nonlinear, it can be written from Kirchhoff's current law as:

$$I = I_{ph} - I_o\left[\exp\left(\frac{q(V+IR_s)}{a\,kT}\right) - 1\right] - \frac{V+IR_s}{R_{sh}} \quad (1)$$

A photocurrent I_{ph} (A) is associated to the photo-generation of electron–hole pairs and equals the short-circuit current if the parasitic resistances are neglected; I_o is the reverse saturation or leakage current of the diode. Furthermore, series and parallel electrical resistances are usually included in the model to represent internal losses; q is the electron charge ($1.60217646 \times 10^{-19}$ C), k is the Boltzmann constant ($1.3806503 \times 10^{-23}$ J/K), T (K) is the temperature of the p–n junction, and a is the diode ideality factor; R_S (Ω) is the series resistance; R_{sh} (Ω) is the shunt resistance.

Due to the transcendental nature of Eq. (1), significant computation effort is required to estimate the model parameters.

Sera et al. [15] developed a five-parameter model, for a PV module and draw the I-V curve based exclusively on the most important parameters from the manufacturers' datasheet (V_{oc}, I_{sc}, I_{mp}, V_{mp}, P_{mp} the current/temperature coefficient μ_{Isc} and the voltage/temperature coefficient μ_{Voc}).

Three equations are used to calculate three unknown parameters (a, R_s and R_{sh}): Eq. (2) is an expression of the I_{mp}, Eq. (3) is written from the derivative of the power with respect to the I_{mp} and Eq. (4) is the derivative of the voltage with respect to the current, at short-circuit current. The system of three equations obtained is solved numerically by an iterative method (e.g. Newton-Raphson or bisection methods). After calculating a, R_s and R_{sh} at STC conditions, the parameters in equations Eqs. (7)–(12) can be inserted in Eq. (1) to get the I-V relationship of the PV module, which takes into account the irradiance and temperature conditions.

Table 1
Implicit and explicit models investigated in this work.

#	Authors	Year	Implicit model	Explicit model	Dependence on the cell temperature	Dependence on the irradiance	Methods	Required parameters
1	Sera el al. [15]	2007	✓		✓	✓	Numerical	a, I_{ph}, I_o, R_s, R_{sh}
2	Villalva et al. [14]	2009	✓		✓	✓	Numerical	I_{ph}, I_o, R_s, R_{sh}
3	Ishaque and Salam [18]	2011b	✓		✓	✓	Numerical	a_1, a_2, I_{ph}, I_o, R_s, R_{sh}
4	Karmalkar and Haneefa [24]	2008		✓			Analytical	m, γ
5	Saloux et al. [26]	2011		✓	✓	✓	Analytical	a, I_{ph}, I_o
6	Das [28]	2011		✓			Analytical	m, n
7	Massi Pavan et al. [13]	2014b		✓	✓	✓	Analytical	m

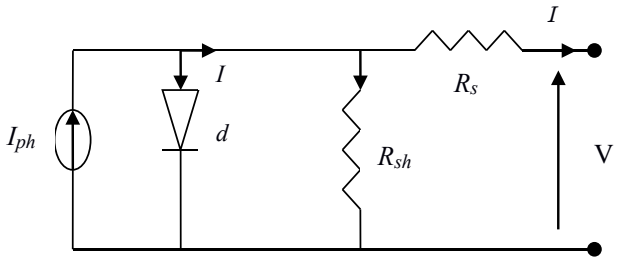

Fig. 1. Equivalent circuit of a photovoltaic cell using the single diode model.

$$I_{mp} = I_{sc} - \frac{V_{mp} - I_{mp}R_s - I_{sc}R_s}{R_{sh}} - \left(I_{sc} - \frac{V_{oc} - I_{sc}R_s}{R_{sh}}\right) e^{-\frac{V_{mp}+I_{mp}R_s-V_{oc}}{N_s V_t}} \tag{2}$$

$$\left.\frac{dP}{dv}\right|_{I=I_{mp}} = I_{mp} + V_{mp} \frac{-\frac{(I_{sc}R_{sh}-V_{oc}+I_{sc}R_s)}{N_s V_t R_{sh}} e^{-\frac{V_{mp}+I_{mp}R_s-V_{oc}}{N_s V_t}} - \frac{1}{R_{sh}}}{1 + \frac{(I_{sc}R_{sh}-V_{oc}+I_{sc}R_s)}{N_s V_t R_{sh}} e^{-\frac{V_{mp}+I_{mp}R_s-V_{oc}}{N_s V_t}} + \frac{R_s}{R_{sh}}} \tag{3}$$

$$\left.\frac{dV}{dI}\right|_{I=I_{sc}} = -\frac{1}{R_{sh}} = \frac{-\frac{(I_{sc}R_{sh}-V_{oc}+I_{sc}R_s)}{N_s V_t R_{sh}} e^{-\frac{I_{sc}R_{sc}-V_{oc}}{N_s V_t}} - \frac{1}{R_{sh}}}{1 + \frac{(I_{sc}R_{sh}-V_{oc}+I_{sc}R_s)}{N_s V_t R_{sh}} e^{-\frac{I_{sc}R_s-V_{oc}}{N_s V_t}} + \frac{R_s}{R_{sh}}} \tag{4}$$

The reverse saturation current I_o and the photocurrent I_{ph} are expressed by Eqs. (5) and (6), respectively.

$$I_o = \left(I_{sc} - \frac{V_{oc} - I_{sc}R_s}{R_{sh}}\right) e^{-\frac{V_{oc}}{N_s V_t}} \tag{5}$$

$$I_{ph} = I_o e^{\frac{V_{oc}}{N_s V_t}} + \frac{V_{oc}}{R_{sh}} \tag{6}$$

$$\begin{aligned} I_{sc}(G) &= I_{sc}G \\ I_{ph}(G) &= I_{ph}G \end{aligned} \tag{7}$$

$$V_{oc}(G) = \ln\left(\frac{I_{ph}(G)R_{sh} - V_{oc}(G)}{I_o R_{sh}}\right) N_s V_t \tag{8}$$

The open-circuit voltage V_{oc} and the short-circuit current I_{sc} depend on the temperature as follows:

$$V_{oc}(T) = V_{oc} + \mu_{v_{oc}}(T - T_{STC}) \tag{9}$$

$$I_{sc}(T) = I_{sc}\left(1 + \frac{\mu_{I_{sc}}}{100}(T - T_{STC})\right) \tag{10}$$

The temperature effect on I_o and I_{ph} can be described by Eqs. (11) and (12), respectively:

$$I_o(T) = \left(I_{sc}(T) - \frac{V_{oc}(T) - I_{sc}(T)R_s}{R_{sh}}\right) e^{-\frac{V_{oc}(T)}{N_s V_t}} \tag{11}$$

$$I_{ph}(T) = I_o(T) e^{\frac{V_{oc}(T)}{N_s V_t}} + \frac{V_{oc}(T)}{R_{sh}} \tag{12}$$

where N_s is the number of solar cells connected in series.

The block diagram for determining the five PV parameters is shown in Fig. 2.

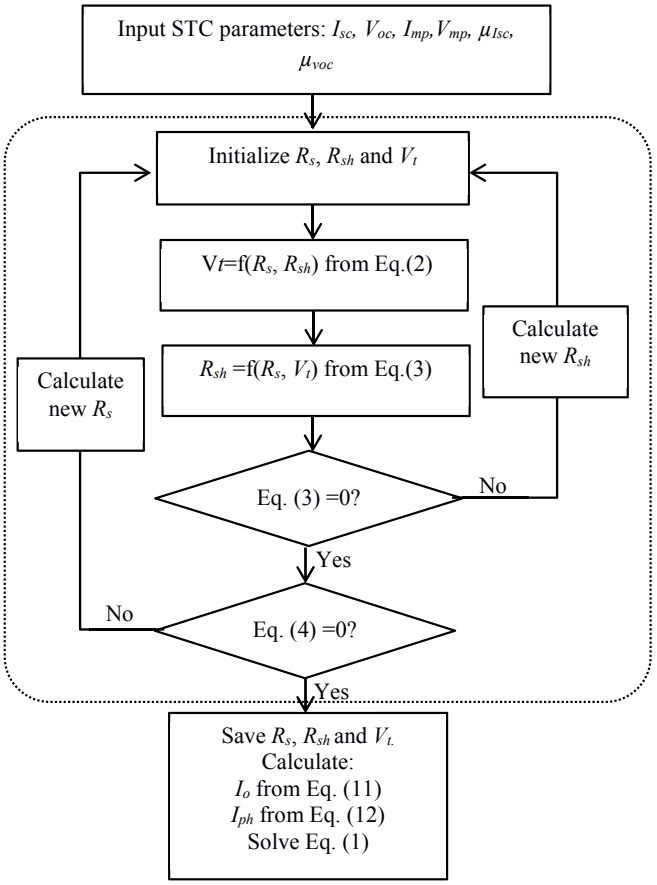

Fig. 2. Block diagram of the model by Sera et al.

2.1.2. Villalva et al. model

The method proposed in Ref. [14] solves the equation of the single-diode model by adjusting the I-V curve at three points: V_{oc}, I_{sc} and P_{mp}. Four unknown parameters in Eq. (1) are needed for the calculation: I_{ph}, I_o, R_s and R_{sh}. The quality factor a of the diode is usually considered as a constant [16], and its value can be later modified in order to improve the model fitting if necessary.

In this model two equations have been introduced:

✓ The first one is the equation for the photocurrent of the PV cell, which depends linearly on the solar irradiation and temperature [15]:

$$I_{ph} = \left(I_{ph,STC} + \mu_{I_{sc}} \Delta T\right) \frac{G}{G_{STC}} \tag{13}$$

Where $I_{ph,STC}$ is photocurrent at STC, $\Delta T = T\text{-}T_{STC}$ (in Kelvin, T_{STC} = 298,15 K), G is the surface irradiance of the cell and G_{STC} (1000 W/m^2) is the irradiance at STC. The constant μ_{Isc} is the short circuit current temperature coefficient, normally provided by the manufacturer.

✓ The second one is the equation for I_o:

$$I_o = \frac{I_{sc,STC} + \mu_{I_{sc}} \Delta T}{e^{\frac{q\left[V_{oc,STC} + \mu_{Voc} \Delta T\right]}{aV_t}} - 1} \tag{14}$$

For calculating R_s and R_{sh} the authors proposed an iterative solution based on the fact that only a unique pair of these two parameters can be obtained by adjusting their values to give a close approximation for the experimental maximum power ($P_{\max,e}$) obtained from the datasheet. Initial guesses for R_s and R_{sh} may be given by:

$$R_{s,\min} = 0$$

$$R_{sh,\min} = \frac{V_{mp}}{I_{sc,STC} - I_{mp}} - \frac{V_{oc,STC} - V_{mp}}{I_{mp}} \tag{15}$$

The expression of R_{sh} is given by:

$$R_{sh} = \frac{V_{mp}\left(V_{mp} + I_{mp}R_s\right)}{V_{mp}I_{ph} - V_{mp}I_o e^{\left(\frac{V_{mp} + I_{mp}R_s}{N_s a}\frac{q}{kT}\right)} + V_{mp}I_{ph} - P_{\max,e}} \tag{16}$$

where: $P_{\max,e}$ is the experimental maximum power obtained from the datasheet.

The calculated maximum power can be computed using:

$$P_{mp} = V_{mp}\left(I_{ph} - I_o\left[\exp\left(\frac{q(V_{mp} + I_{mp}R_s)}{a\,kT}\right) - 1\right] - \frac{V_{mp} + I_{mp}R_s}{R_{sh}}\right) \tag{17}$$

The model may be further improved by exploiting the iterative solution of R_s and R_{sh}. Thus, a new relation between I_{sc} and I_{ph} at STC conditions is introduced:

$$I_{ph,STC} = \frac{R_{sh} + R_s}{R_{sh}} I_{sc,STC} \tag{18}$$

The block diagram for determining the four PV parameters is presented in Fig. 3.

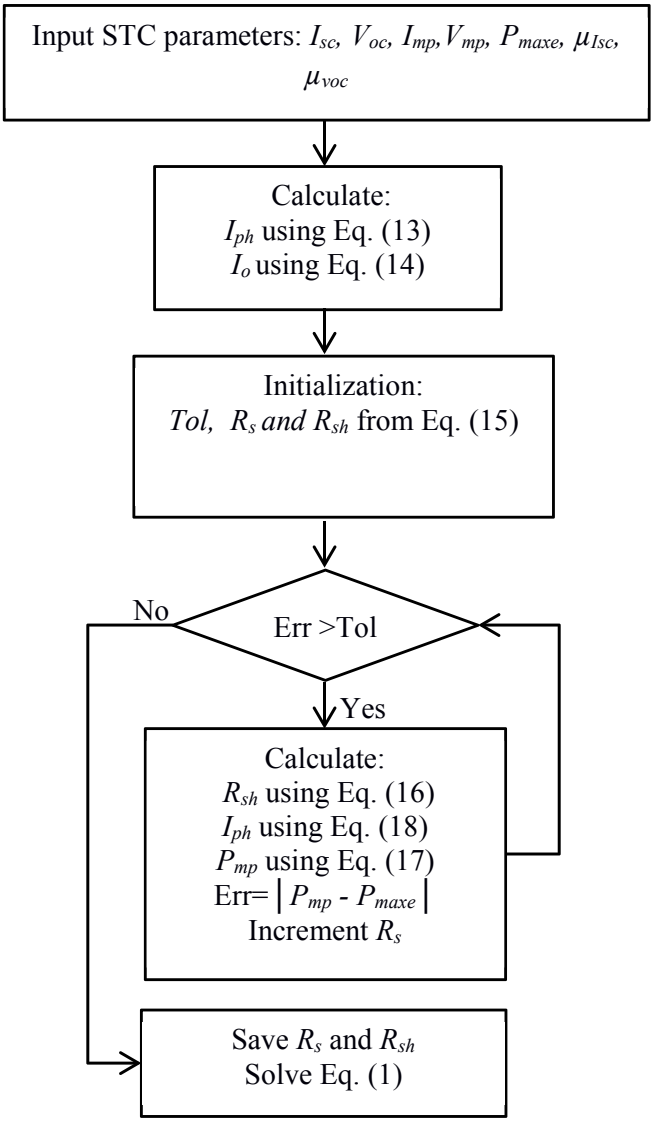

Fig. 3. Block diagram of the model by Villalva et al.

2.1.3. Ishaque and Salam model

Ishaque and Salam [18] present a two-diode model of the solar cell where the equivalent circuit is presented in Fig. 4 and the output current is described by the following equation:

$$I = I_{ph} - I_{o1}\left[\exp\left(\frac{q(V + IR_s)}{a_1\,kT}\right) - 1\right] - I_{o2}\left[\exp\left(\frac{q(V + IR_s)}{a_2\,kT}\right) - 1\right] - \frac{V + IR_s}{R_{sh}} \tag{19}$$

Here I_{o1} (A) is the dark saturation current due to recombination in the quasi-neutral region; I_{o2} (A) is the dark saturation current due to recombination in the space-charge region; a_1 and a_2 are the ideality factors of the diodes. The two-diode model requires computation of seven parameters (I_{ph}, R_s, R_{sh}, I_{o1}, I_{o2} a_1 and a_2) that variously affect the shape of the I–V characteristics.

Ishaque and Salam [18] use the same expression described in Ref. [14] (Eq. (13)) to calculate the photocurrent. However, a new analytical equation of both saturation currents is derived: I_{o1}, I_{o2} are set to be equal in magnitude and can be calculated as:

$$I_{o1} = I_{o2} = I_o = \frac{I_{sc,STC} + \mu_{I_{sc}} \triangle T}{e^{\frac{q\left[V_{oc,STC} + \mu_{Voc} \Delta T\right]}{\left[(a_1 + a_2)/p\right]V_t}} - 1} \tag{20}$$

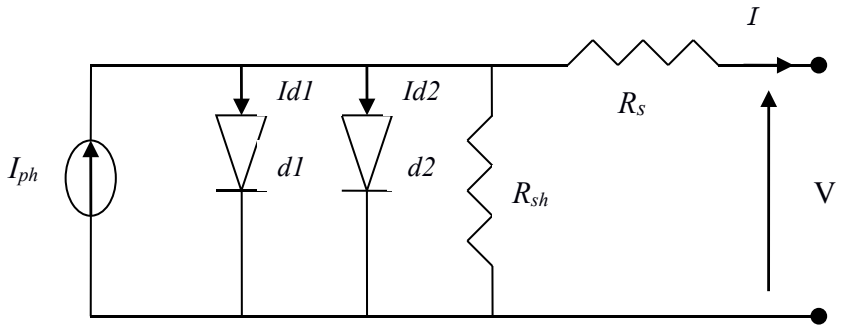

Fig. 4. Equivalent circuit of a photovoltaic cell using the two-diode model.

According to Ishaque and Salam [18], a_1 must be unity while the value of a_2 is flexible. It is found that the best match between the proposed model and the experimental I–V curve can be observed if $a_2 \geq 1.2$. Since $(a_1 + a_2)/p = 1$ and $a_1 = 1$, the variable p can be chosen as $P \geq 2.2$.

To calculate R_s and R_{sh} the authors applied the same approach used for the single diode model reported in Ref. [14]. The initial conditions for both resistances are the same given in Ref. [14]. The expression of R_{sh} was rearranged and rewritten to be applied in the model by introducing p and the two exponentials terms as given in Eq. (21):

$$R_{sh} = \frac{V_{mp} + I_{mp}R_s}{I_{ph} - I_o \left(e^{\left(\frac{V_{mp}+I_{mp}R_s}{V_t}\right)} + e^{\left(\frac{V_{mp}+I_{mp}R_s}{(p-1)V_t}\right)} + 2 \right) - \frac{P_{\max.e}}{V_{mp}}} \tag{21}$$

With the availability of all six parameters, the output current of the module can be determined using the standard Newton-Raphson method. The block diagram presented in Fig. 5 describes the procedure for calculating the PV parameters.

2.2. Explicit models

2.2.1. Karmalkar and Haneefa model

An explicit model is presented in Ref. [24], allowing the prediction of the entire I–V curve from four measurements of the curve corresponding to *Voc*, ~0.6 *Voc*, *Isc*, and ~0.6 *Isc*. The model provides a closed-form description of the I–V curve, peak power point, and fill factor in terms of physical parameters of the single exponential model. The normalization of i and v ($i = V/Voc$ and $v = I/Isc$) enables a compact representation of the I–V measurements for a wide variety of cells in which recombination, tunnelling, or space charge-limited currents may exist in addition to diffusion. The empiric expression of the model is written as [24]:

$$i = 1 - (1 - \gamma)v - \gamma v^m \tag{22}$$

Two parameters (m and γ) should be extracted by using two additional simple measurements of i for $v = 0.6$ and v for $i = 0.6$. Thus, γ is approximated from Eq. (23), while m can be calculated from Eq. (24):

$$\gamma \approx (i|_{v=0.6} - 0.4)/0.6 \tag{23}$$

$$m = \log\left[(0.4 - (1 - \gamma)v|_{i=0.6})\gamma^{-1}\right] \Big/ \log v|_{i=0.6} \tag{24}$$

Closed-form solutions for the (i_p,v_p) point and FF are derived from Eq. (22). The normalized peak power voltage $v_p = V_p/V_{oc}$ is obtained by setting: $d(iv)/dv|_{v=v_p} = 0$, v_p can be empirically adjusted

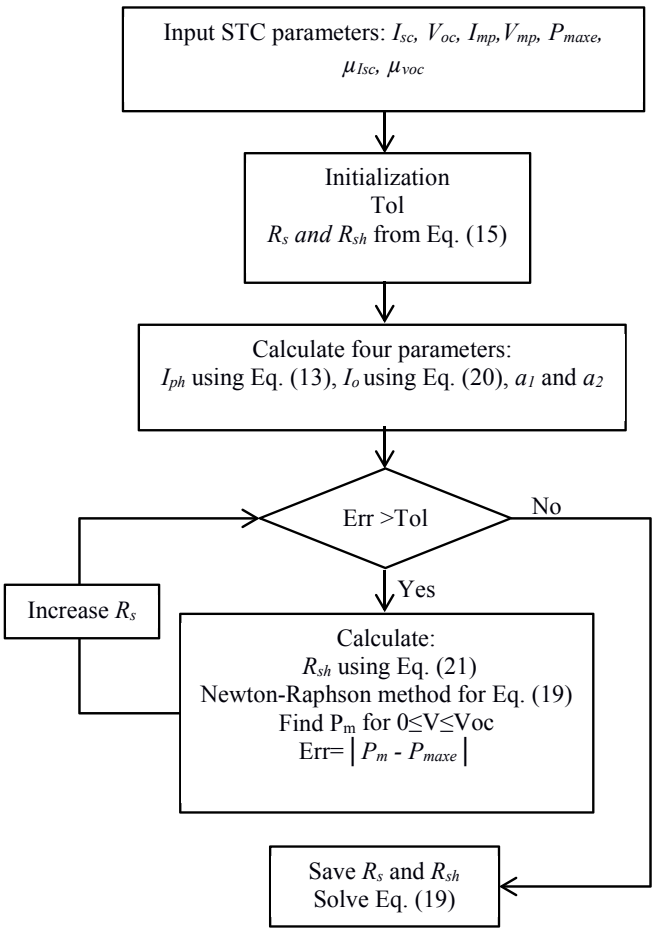

Fig. 5. Block diagram of the model by Ishaque and Salam.

as:

$$v_p \approx (m + 1)^{-1/m} - 0.05(1 - \gamma) \tag{25}$$

The *FF* is given by:

$$FF = v_p i_p = v_p \left[1 - (1 - \gamma)v_p - \gamma v_p^m\right] \tag{26}$$

To avoid the measurement of *dI/dV* slopes and peak power point, the physical parameters a, R_s, I_o, R_{sh}, and I_{ph} of the single diode model can be extracted using the following closed-form expressions [27]:

$$a \approx \frac{V_{oc}}{mV_t}\left(\frac{0.77m(1-v_p)-1}{0.77m\ln\left(\frac{1}{v_p}\right)-1}\right) \tag{27}$$

$$R_s \approx \left(\frac{V_{oc}}{0.6\gamma m I_{sc}}\right)\left(1-\frac{amV_t}{V_{oc}}\right)-0.1 \tag{28}$$

$$I_o \approx \gamma I_{sc} e^{-\frac{V_{oc}}{aV_t}} \tag{29}$$

$$R_{sh} \approx \left(\frac{V_{oc}}{I_{sc}}\right)\left(1-\gamma-\frac{\gamma}{0.6}\exp\left(\frac{(0.4+0.6\gamma)I_{sc}R_s-0.4V_{oc}}{aV_t}\right)\right)^{-1} \tag{30}$$

$$I_{ph} \approx \frac{I_{sc}}{(1+R_s/R_{sh})^{-1}} \tag{31}$$

The block diagram for computing the different parameters is shown in Fig. 6. The model validation is established for a limited class of cells, having moderately convex I–V curves with *FFs* of 0.56–0.77 and obeying the single-diode exponential model with bias-independent photocurrent. The scope of the explicit model [24] is expanded in Ref. [29] to cover cells having a wide range of material systems from concave ($FF < 0.25$) to highly convex ($FF > 0.85$).

2.2.2. Saloux et al. model

A single-diode model without series and shunt resistances is introduced by Saloux et al. [26]. The standard I-V Eq. (32) is used.

$$I = I_{ph} - I_o\left[\exp\left(\frac{qV}{aN_skT}\right)-1\right] \tag{32}$$

Considering the asymptotic behaviour of the I–V curve at short and open circuit conditions, the derivative of the current in correspondence of the maximum power is calculated as [26]:

$$\left.\frac{dI}{dV}\right|_{Vmp} \cong -\frac{I_{sc}}{V_{oc}} \tag{33}$$

Explicit Eqs. (34)–(37) are used directly to calculate the electrical parameters (V_{mp}, I_{mp} and P_{mp}) at the maximum power point as function of both cell temperature and irradiance.

$$V_{mp} = \frac{nN_sk_bT}{q}\ln\left[\frac{nN_skT}{qI_0}\ \frac{I_{sc}}{V_{oc}}\right] \tag{34}$$

$$I_{mp} = I_{ph} + I_o - \frac{nN_skT}{q}\left(\frac{I_{sc}}{V_{oc}}\right) \tag{35}$$

$$P_{mp} = I_{mp}V_{mp} \tag{36}$$

The ideality factor a is calculated by the following equation [26]:

$$a = \frac{q(V_{mp}-V_{oc})}{N_skT}\left[\ln\left(1-\frac{I_{mp}}{I_{sc}}\right)\right]^{-1} \tag{37}$$

I_{ph} and I_o can be calculated using Eqs. (13) and (14), respectively. The block diagram for calculating the different PV parameters is depicted in Fig. 7.

2.2.3. Das model

In Ref. [28], an approach is presented in order to find a closed-form solution for V_{mp}, I_{mp} and *FF*. The model is mainly based on the method introduced in Ref. [24]. The explicit expression of the model is determined as [28]:

$$v^m + i^n = 1 \tag{38}$$

I_{sc} and V_{oc} are measured directly, m and n are extracted using two additional measurement of i for two any values of v lies in $(0,1)$. From Eq. (38) the author states that:

$$\log n \log i = \log(1-v^m) \approx -v^m \tag{39}$$

So, a measurement of j at $(v=a)$ and $(v=b)$ leads to:

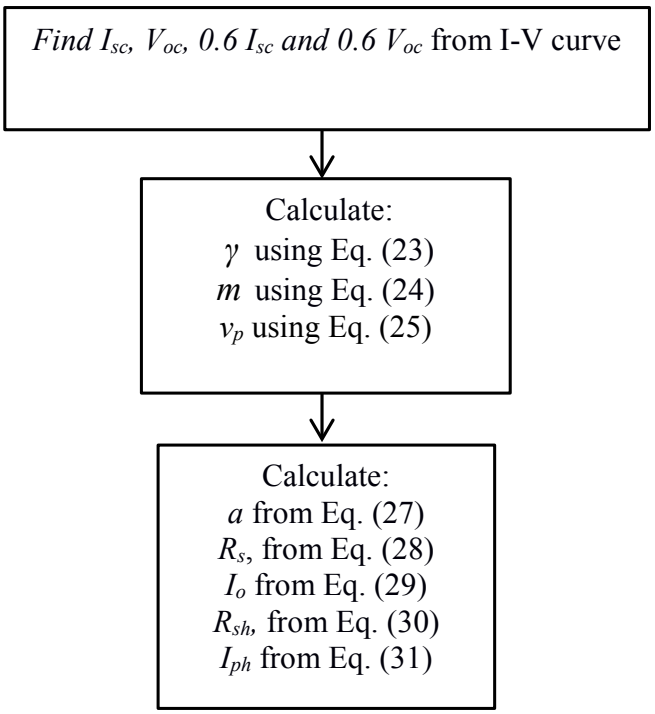

Fig. 6. Bloc diagram of the model proposed by Karmalkar and Haneefa.

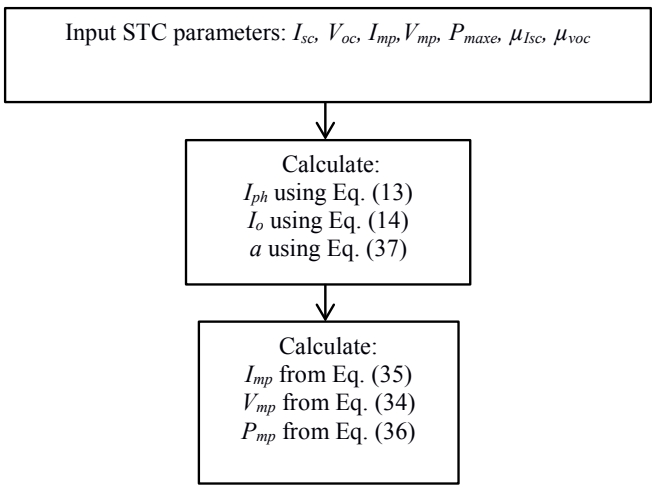

Fig. 7. Block diagram of the model by Saloux et al.

$$m \approx \frac{\log\left(\frac{\log i_a}{\log i_b}\right)}{\log\left(\frac{a}{b}\right)} \tag{40}$$

Thus, n can be approximated as:

$$n \approx \frac{-a^m}{\log i_a} \tag{41}$$

To find the values of m and n, $a = 0.8$ and $b = 0.9$ are used for a satisfactory result. The normalized maximum power voltage v_{mp} is obtained from Eq. (42), and the FF is consequently calculated using Eq. (43).

$$v_{mp} = \left(1 + \frac{m}{n}\right)^{-(1/m)} \tag{42}$$

$$FF = v_{mp} i_{mp} = \left(\frac{m}{n}\right)^{1/n} \left(1 + \frac{m}{n}\right)^{-\left(\frac{1}{m}+\frac{1}{n}\right)} \tag{43}$$

The procedure for computing the two parameters (n and m) and estimating v_{mp} and FF is presented in Fig. 8.

This model is useful for the design, characterization and calculation of the fill factor, its applicability was demonstrated with the measured data of a wide variety of solar cells, (i.e. Si, CdTe, GaAs/Ge, a-SiC:H/c-Si). However, this model is intuitive and lacks analytical support. A new analytical explicit I–V model is introduced in Ref. [31], which is derived from the physics based on the implicit I–V equation.

2.2.4. Massi Pavan et al. model

In Refs. [3,13,32,33] the authors developed an explicit empirical model, where the electrical parameters listed in the datasheets or in the flash tests of any photovoltaic module are sufficient to describe its behaviour. For a PV module, the model is defined by the following equation:

$$I = I_L + z\Delta T - \frac{e^{m\cdot[V - w\Delta T]} - 1}{e^m - 1} \tag{44}$$

where I (p.u.) is the per unit current referred to the short circuit current I_{sc} (A) at STC, I_L (p.u.) is the per unit irradiance referred to 1.000 W/m^2, m is an exponential factor, V (p.u.) is the per unit voltage

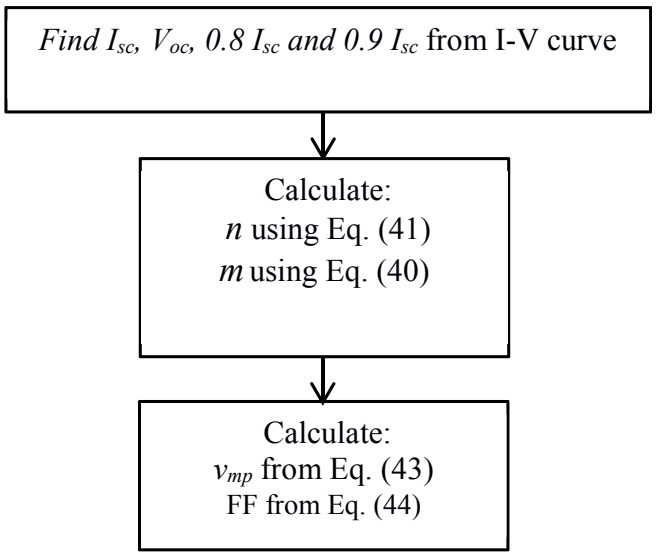

Fig. 8. Bloc diagram of the model by Das.

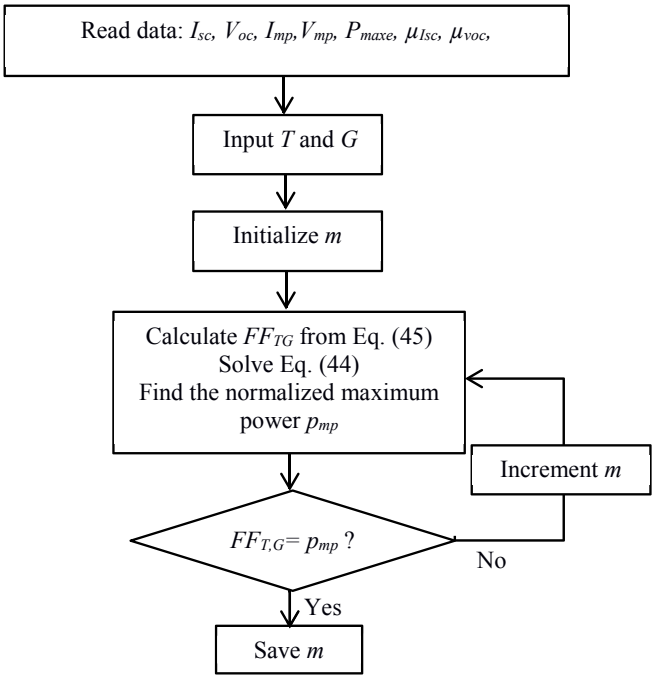

Fig. 9. Block diagram of the model proposed by Massi Pavan et al.

referred to the open circuit voltage at STC V_{oc} (V), z (1/°C) is the current-temperature coefficient referred to the short circuit current at STC ($z = \mu_{Isc}/I_{sc}$), w (1/°C) is the voltage-temperature coefficient referred to the open circuit voltage at STC ($w = \mu_{Voc}/V_{oc}$), $\Delta T = (T\text{-}25)$ °C is the temperature difference with respect to the standard temperature (25 °C), and T (°C) is the solar cell temperature.

The exponential factor m is obtained imposing that the maximum power produced by the photovoltaic module at a given irradiance and solar cell temperature is equal to its fill factor.

The fill factor $FF_{T,G}$ can be calculated by the following empirical equation:

$$FF_{T,G} = FF_{0,T} \cdot (1 - r_{S,GT}) \tag{45}$$

where $r_{s,GT}$ is the normalized series resistance at a cell temperature T and irradiance G, as presented in Eq. (46):

$$r_{s,GT} = \frac{I_{SC,G}}{V_{OC,T}} \cdot R_s \tag{46}$$

where R_s is the series resistance, $V_{oc,T}$ can be calculated form Eq. (9) and $I_{sc,G}$ is expressed as follows:

$$I_{SC,G} = \frac{G}{1000} \cdot I_{SC} \tag{47}$$

Table 2
Electrical parameters of the used PV modules.

Technology	m-Si	CIGS	CdTe
Module	Q.Pro 230	Q.Smart UF 95	Fs-272
Nominal power P_n (W)	230	95	72.5
Short circuit current I_{SC} (A)	8.30	1.68	1.23
Open circuit voltage V_{OC} (V)	36.61	78.0	88.7
Current at maximum power point I_m (A)	7.84	1.53	1.09
Voltage at maximum power point V_m (V)	29.56	62.1	66.6
Current/temperature coefficient Z (%/K)	+0.04	0.00	0.04
Voltage/temperature coefficient W (%/K)	−0.41	−0.38	−0.25
Number of cells in series	60	116	116

$FF_{0,T}$ is the normalized fill factor at a cell temperature T, it can be expressed as:

$$FF_{0,T} = \frac{v_{OC,T} - \ln(v_{OC,T} + 0.72)}{v_{OC,T} + 1} \quad (48)$$

where $v_{OC,T}$ ( ) is the normalized open circuit voltage $V_{oc,T}$, which may be calculated as:

$$v_{OC,T} = \frac{V_{OC,T}}{V_t \cdot N_s} \quad (49)$$

A more detailed description of the fill factor calculations is presented in Ref. [3]. The block diagram for computing the exponential factor m is depicted in Fig. 9.

3. Comparative study

The explicit and implicit models presented in the previous

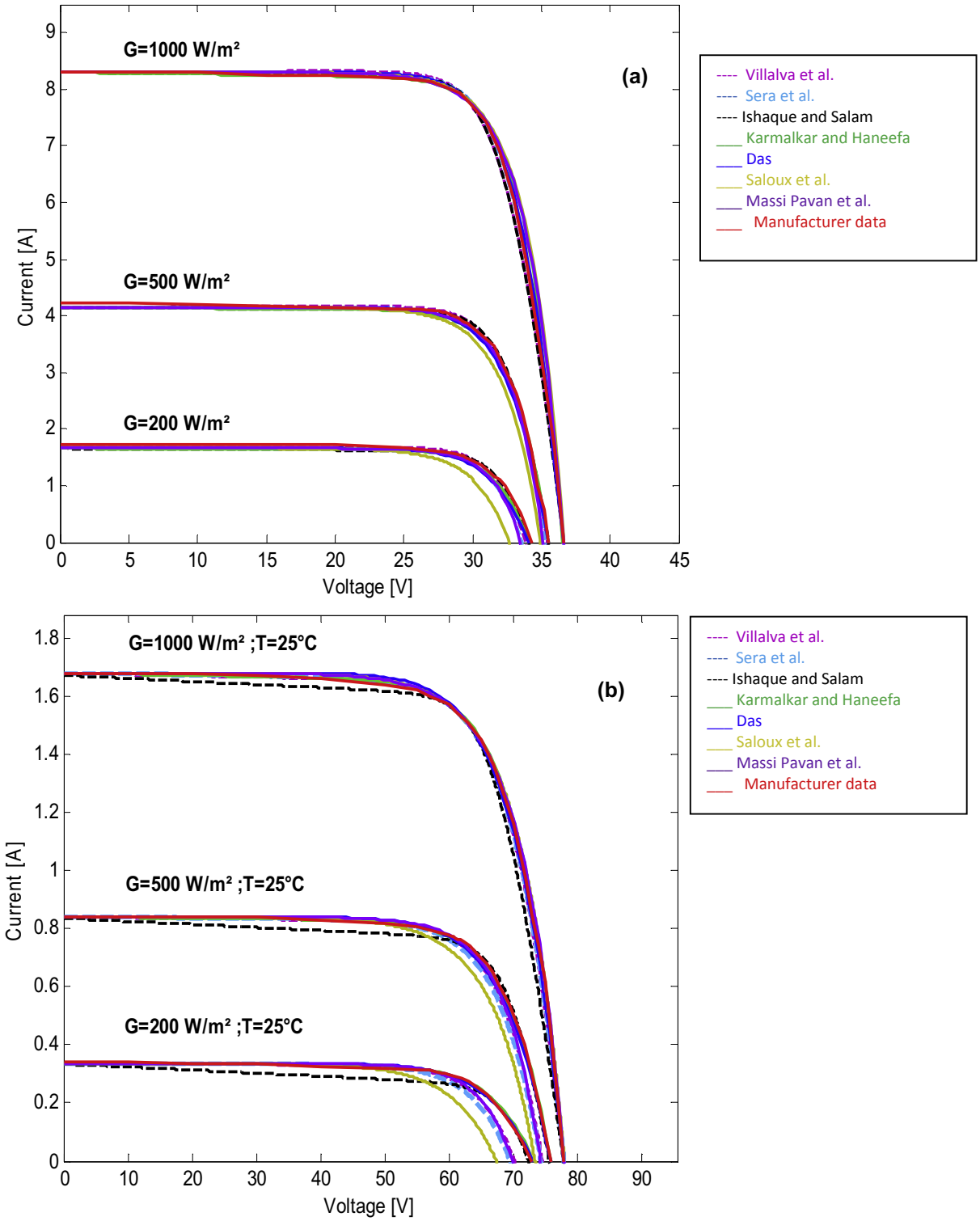

Fig. 10. Test 1: I-V characteristics: (a) Q.pro230 PV module at different irradiance levels (b) Q.Smart UF95 PV module at different irradiance levels.

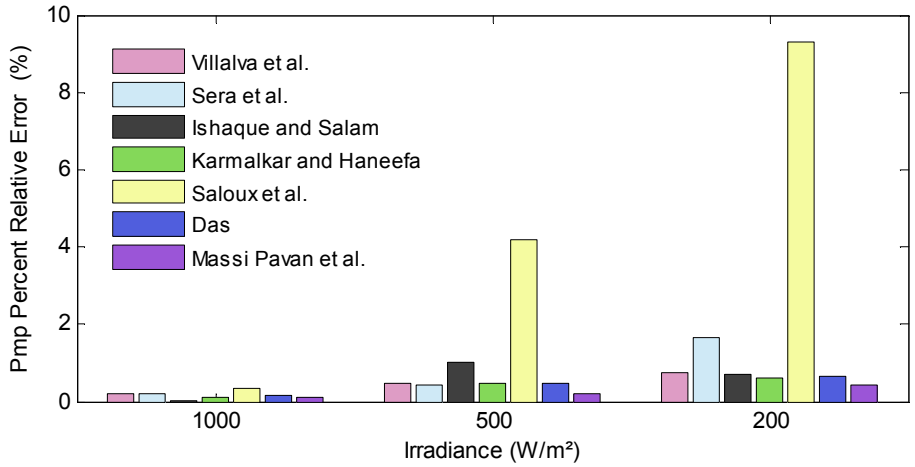

(a)

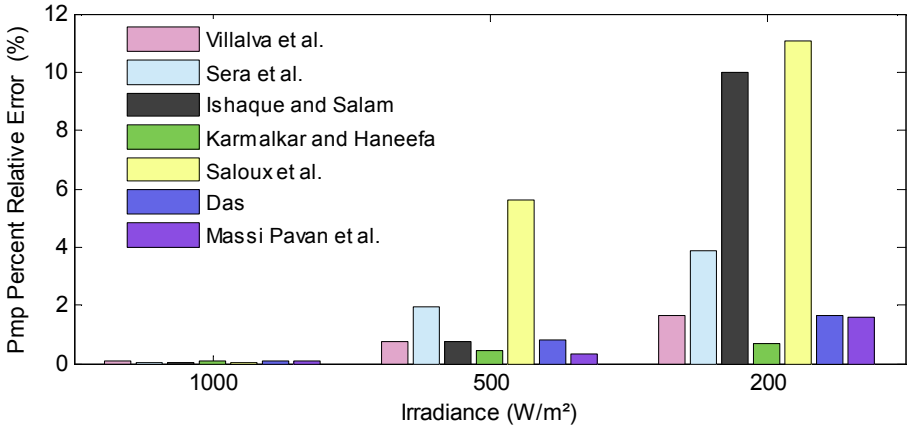

(b)

Fig. 11. Test 1: Percentage relative errors at MPP: (a) Q.Pro 230 module, (b) Q.Smart module.

Table 3a
Q.Pro230 PV module: Parameters calculated at STC conditions (Test 1).

Parameters	Villalva et al.	Sera et al.	Ishaque and Salam	Karmalkar and Haneefa	Saloux et al.	Das	Massi Pavan et al.
a( )	1.3	1.1	1.35	1.42	1.58	–	–
$R_s(\Omega)$	0.22	0.4	0.31	0.43	–	–	–
$R_{sh}(\Omega)$	257.72	1627.98	694.972	549.17	–	-	–
$I_{ph}(A)$	8.29	8.3	8.3	8.3	8.3	–	–
$I_o(A)$	9.77e-8	3.10e-8	3.98e-10	4.34e-7	2.48e-6	–	–
m( )	–	–	–	13.79	–	14.14	14.7
n( )	–	–	–	–	–	0.84	–
γ ( )	–	–	–	0.99	–	–	–
$I_{sc}(A)$	8.3	8.3	8.3	8.3	8.3	8.3	8.3
$V_{oc}(V)$	36.6	36.5	36.5	36.58	36.6	36.61	36.61
$I_{mp}(A)$	7.84	7.76	7.80	7.71	7.75	7.71	7.71
$V_{mp}(V)$	29.50	29.80	29.70	30.02	30.01	30.01	30.02

section are implemented in Matlab® environment and applied to actual commercial PV modules belonging to different PV technologies: Q.Pro230 [34], Q.Smart UF95 [35] and First Solar FS-272 [36]. In order to compare and assess the accuracy of the models, the estimated I-V curves are compared with the manufacturer's data and with some experimental measurements. The specifications of the used PV modules are summarized in Table 2.

3.1. Comparing estimated and manufacture's data (test 1)

The investigated models have been tested by comparing their output with some parameters listed in the datasheet of Q.Pro230 and Q.Smart UF95. Fs-272 has not been used in Test 1 because the manufacturer does not provide the necessary I-V curves.

With reference to Figs. 10 and 11, at STC all studied models

Table 3b
Q.Smart UF-95 PV module: Parameters calculated at STC conditions (Test 1).

Parameters	Villalva et al.	Sera et al.	Ishaque and Salam	Karmalkar and Haneefa	Saloux et al.	Das	Massi Pavan et al.
a( )	1.6	1.75	1.6	1.8	2.2	–	–
$R_s(\Omega)$	2.16	1.72	4.39	1.37	–	–	–
$R_{sh}(\Omega)$	2149.44	3113.63	942.59	2338.8	–	-	–
$I_{ph}(A)$	1.68	1.68	1.68	1.68	1.68	–	–
$I_o(A)$	1.33e-7	5.39e-7	7.13e-12	8.69e-7	1.19e-5	–	–
m( )	–	–	–	11.38	–	10.87	11.8
n( )	–	–	–	–	–	0.94	–
γ ( )	–	–	–	0.98	–	–	–
$I_{sc}(A)$	1.68	1.68	1.67	1.68	1.68	1.68	1.68
$V_{oc}(V)$	77.8	77.9	77.8	77.96	77.9	78	78
$I_{mp}(A)$	1.529	1.529	1.527	1.524	1.520	1.543	1.521
$V_{mp}(V)$	62.20	62.10	62.20	62.37	62.52	61.62	62.40

Table 4
Maximum power for each module at Tc = 25 °C and different solar irradiance levels (Test 1).

Module	Extracted P_{mp} (W)	Villalva et al.	Sera et al.	Ishaque and Salam	Karmalkar and Haneefa	Saloux et al.	Das	Massi Pavan et al.
Q.Pro230								
G = 200 W/m^2	44.68	44.34	45.42	45	44.41	40.53	44.38	44.49
G = 500 W/m^2	114.62	114.08	115.11	115.80	114.09	109.83	114.09	114.37
G = 1000 W/m^2	231.75	231.28	231.24	231.66	231.45	232.57	231.38	231.49
Q.Smart UF 95								
G = 200 W/m^2	17.78	17.49	17.09	16.00	17.90	15.81	17.49	17.50
G = 500 W/m^2	46.67	46.31	45.75	46.32	46.45	44.06	46.29	46.51
G = 1000 W/m^2	95.01	95.10	94.95	94.97	95.10	95.04	95.08	94.94

Table 5
relative errors between estimated and provided MPP in the Datasheet (Test 1).

Modules	Villalva et al.	Sera et al.	Ishaque and Salam	Karmalkar and Haneefa	Saloux et al.	Das	Massi Pavan et al.
Q.Pro230							
1000 W/m^2	0.20	0.22	0.03	0.13	0.35	0.16	0.11
500 W/m^2	0.47	0.43	1.03	0.46	4.17	0.46	0.21
200 W/m^2	0.76	1.65	0.71	0.60	9.28	0.67	0.43
Mean PRE(%)	0.48	0.77	0.59	0.39	4.6	0.43	0.25
Q.SmartUF95							
1000 W/m^2	0.09	0.06	0.04	0.09	0.03	0.07	0.07
500 W/m^2	0.77	1.97	0.75	0.47	5.59	0.81	0.34
200 W/m^2	1.63	3.88	10.01	0.67	11.07	1.63	1.57
Mean PRE(%)	0.83	1.97	3.6	0.41	5.57	0.83	0.66

predict, with a good degree of approximation, the data provided by the manufacturer. In particular, the predicted maximum power is very accurate. The performance of the models became poorer when the irradiance decreases. In particular, there are some differences between the forecasted and the provided maximum power and open circuit voltages. A small difference is also present in the case of the short circuit current, but this is quite small.

Tables 3a and 3b show the electrical parameters calculated for each model at STC conditions. The maximum powers from the datasheets and the application of the models are reported in Table 4, while Fig. 2 and Table 5 present the Percentage Relative Errors (PRE) for the different levels of solar irradiance.

$$PRE(\%) = \frac{\left|P_{mp,measured} - P_{mp,estimated}\right|}{P_{mp,measured}} 100 \quad (50)$$

With reference to the presented PREs and the I-V curves, the following remarks are worth mentioning:

- All models perform pretty well at STC;
- With reference to the Q.Pro module, the model Massi Pavan et al. presents the best average performances (the mean PRE is 0.43%), while the worst are the ones provided by the Saloux et al. model (the mean PRE is 4.6%);
- With reference to the Q.Smart module, the model Kamalkar and Haneefa presents the best average performances (the mean PRE is 0.41%), while the worst are the ones provided by the Saloux et al. model (the mean PRE is 5.57%);
- The performances of the studied models are worst for low irradiances.

3.2. Comparing estimated and experimental data (test 2)

A number of measurements have been carried out at the test facility of the University of Trieste, Italy. Trieste has a temperate climate, with hot summers, mild winters and no dry season. Over the course of a year, the temperature typically varies from 4 °C to 29 °C. The relative humidity typically ranges from 45% to 84% while the average wind speed ranges between 2 m/s and 5 m/s – although very strong winds are common for short periods of time [37].

Fig. 12 shows the PV modules, the data loggers for climatic and electrical data, and the electrical equipment (a DC–DC converter, a heat sink and a load) of the test facility at the University of Trieste,

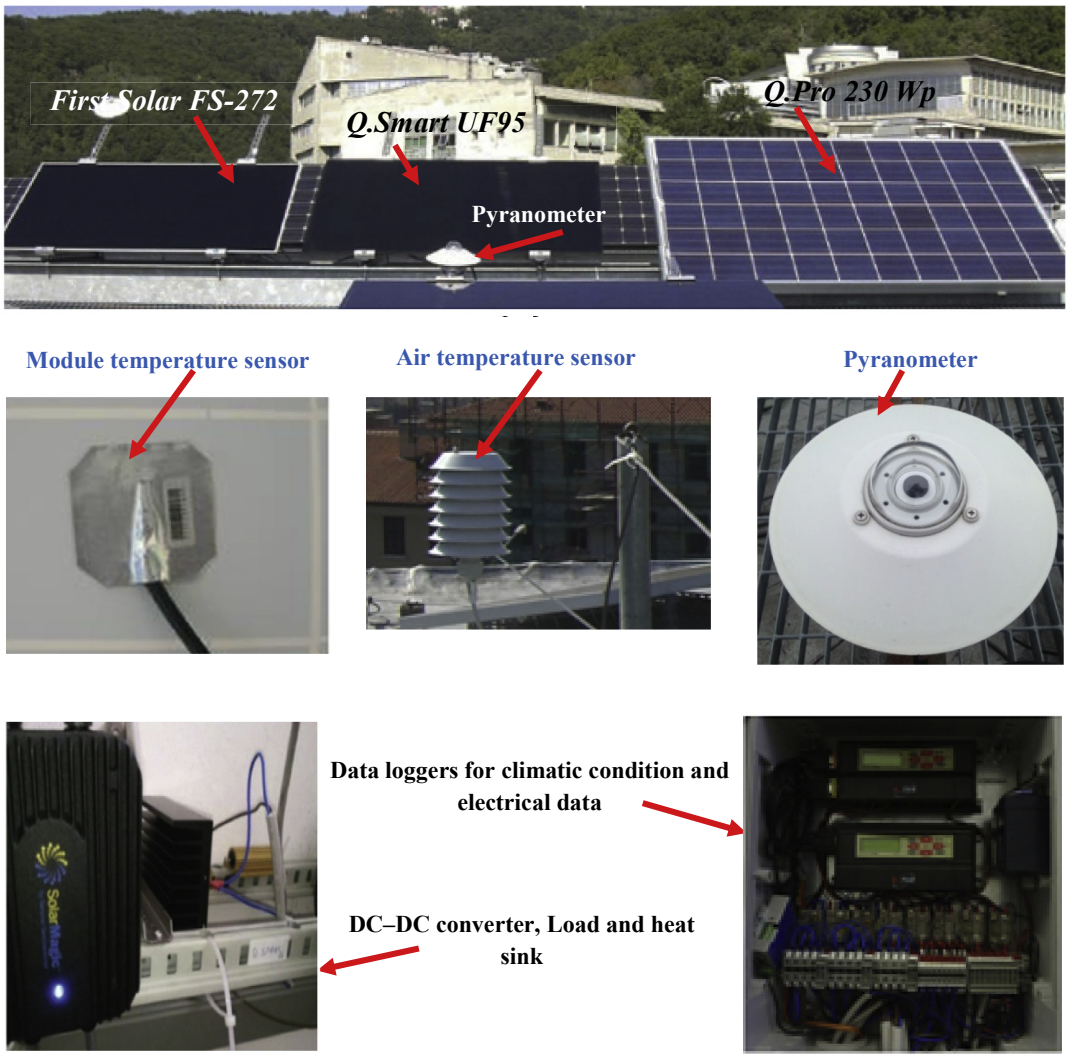

Fig. 12. The examined PV modules and the test facility (University of Trieste, Italy).

Table 6
Date, time and operating conditions for each PV module.

Module	Date	Time (hh:mm)	Ambient temperature Ta(°C)	Cell temperature T(°C)	Global Irradiance G(W/m^2)
Q.Pro 230	03/09/2013	11:45	32	57	906
	03/09/2013	09:13	32	37	479
	18/09/2013	17:02	23.44	28	135
Q.Smart UF95	12/03/2014	12:21	16	35	800
	13/03/2014	09:30	14	21	490
	26/03/2014	17:25	10	11	127
First Solar FS-272	27/09/2013	17:10	10	12	106
	05/09/2013	09:05	26.7	40.9	509
	05/09/2013	11:50	27.18	53.47	997

where the experimental measurements have been carried out.

Each photovoltaic module transfers electrical power to the load (a resistor) through the DC–DC converter – *type Solar Magic produced by National Semiconductor Ltd*. The part of the monitoring system used in the test consists of: two data loggers *E-Log, MW8024-02/10* produced by *LSI Lastem S.r.l.*(all the characteristics of this device can be found in Ref. [38]), one used for the climatic data and one for the electrical ones; one laptop connected to the two data-loggers where the data are being collected in a database; one *ISO9060* first class thermopile global radiometer type *C100R DPA153* produced by *LSI Lastem S.r.l.* installed on the same plane of the photovoltaic modules (the daily uncertainty for this device is less than 5%, the sensitivity is 30÷45 μV/W/m^2 and the flat spectral response range is (305–2800 nm), more information about the device can be found in Ref. [38]); three module temperature contact probes type *DLE 124* produced by *LSI Lastem S.r.l* (the accuracy of this device is ±0.15 °C, more details can be found in Ref. [38]); three shunts type *SHP300A60-Compact* produced by *Hobut Ltd.* (the

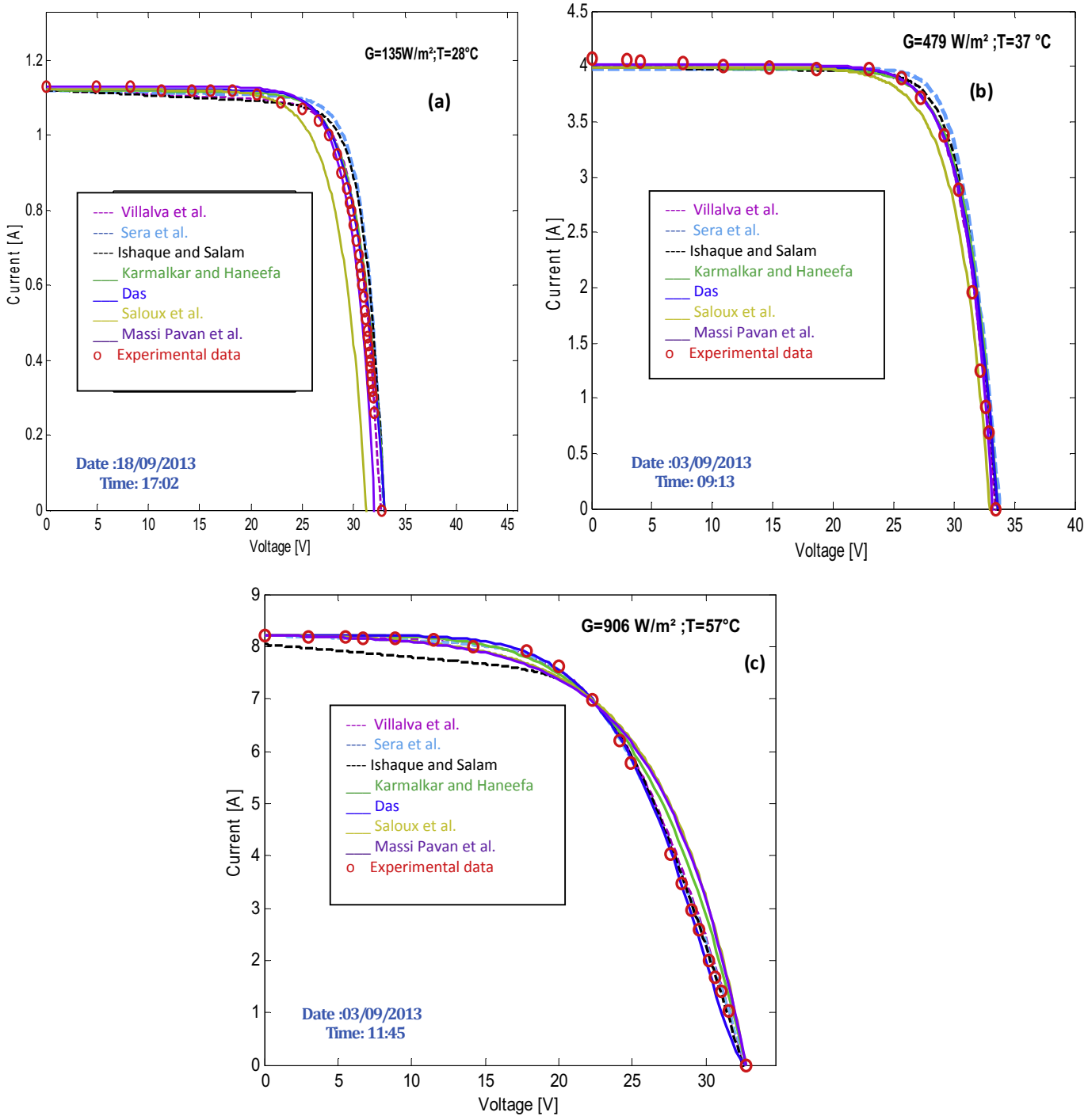

Fig. 13. Test 2: Measured vs simulated I-V characteristics of Q.Pro230 PV module at (a) low irradiance, (b) medium irradiance and (c) high irradiance.

characteristics of this instrument can be found in Ref. [39]) that have been calibrated with an accuracy better than 0.01%.

Three different PV modules employed at different operating conditions of global solar irradiance (low, medium and high), ambient temperature and cell's temperature have been used. The investigated modules, as well as the operating conditions are listed in Table 6.

The experimental and the simulated I-V curves of each module are illustrated in Figs. 13–15. The maximum power point for each module and the percentage relative error are reported in Tables 7a–7c).

With reference to the aforementioned results, the following remarks can be made:

- All models show a good performance for Q.Pro 230 module. The model Karmalkar and Haneefa gives the smallest error in the calculation of the maximum power at high and medium solar irradiance ((0.06 ± 0.01)% and (0.5 ± 0.02)% respectively), while the model by Massi Pavan et al. [13] gives the smallest error at low irradiance ((1.20 ± 0.05)%);
- With reference to Q.Smart UF95 module operating at high values of solar irradiance, all models perform well. At low and

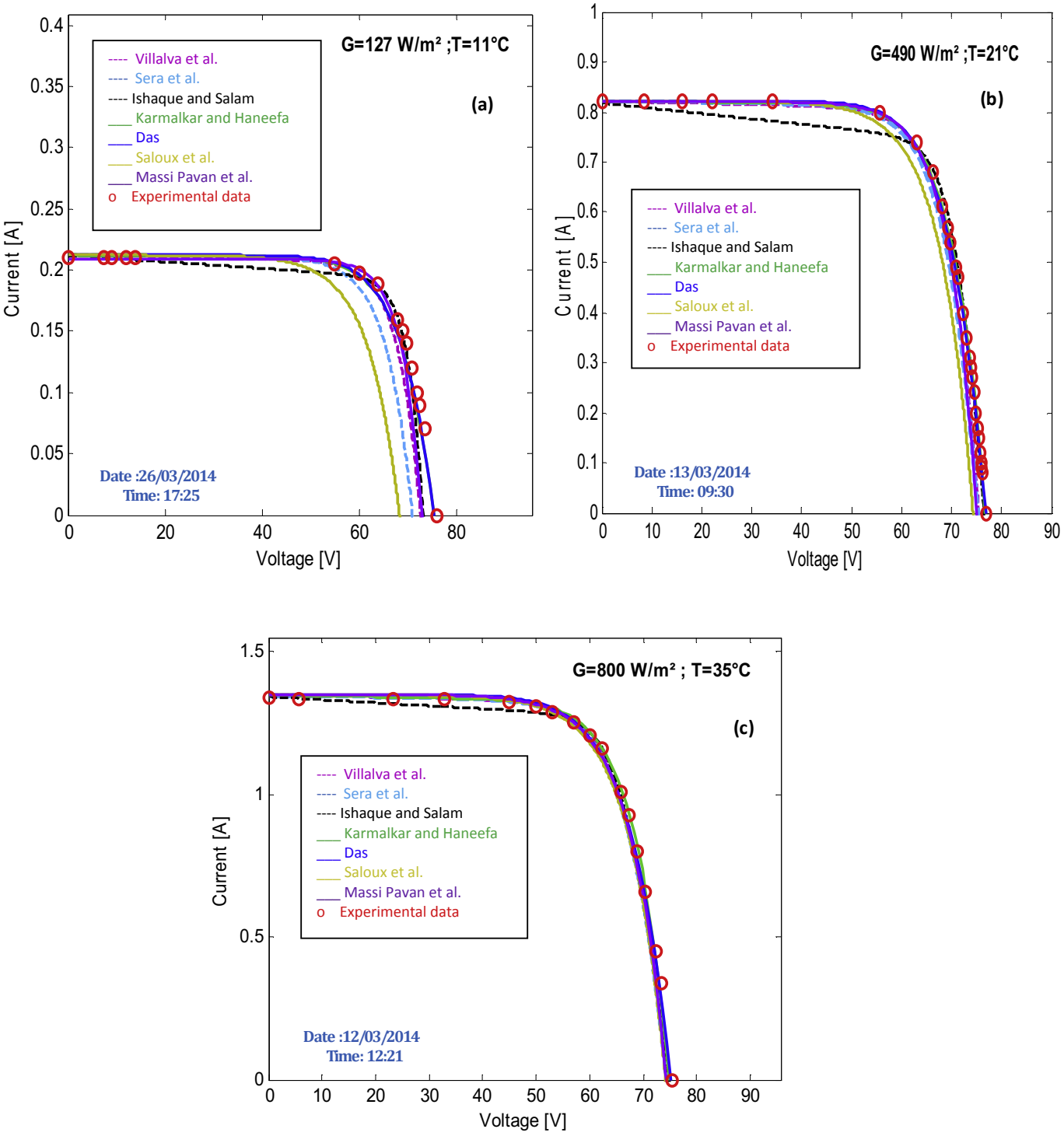

Fig. 14. Test 2: Measured vs simulated I-V characteristics of Q.Smart UF95 PV module at (a) low irradiance, (b) medium irradiance, and (c) high irradiance.

medium irradiance only the models developed by Massi Pavan et al., Karmalkar and Haneefa, and Das give good results along the entire I-V curve. With reference to the maximum power point, the smallest error ((0.24 ± 0.01)%) is obtained with the model by Massi Pavan et al.;

- Concerning the FS-272 operating at higher value of solar irradiance, all models show good performance except the one proposed by Ishaque and Salam and by Saloux et al. The model by Massi Pavan et al. [13] presents the smallest error of (0.46 ± 0.02) % at maximum power point. The model by Karmalkar and Haneefa shows also a good performance with an error of (0.57 ± 0.02) % at maximum power point. At low and medium irradiance, again models by Massi Pavan et al. [13] and Karmalkar and Haneefa [24] provide the most accurate prediction at maximum power point. However, at low irradiance only the models by Karmalkar and Haneefa [24] and Das [28] show good agreement with the measurements along the entire I-V curve.

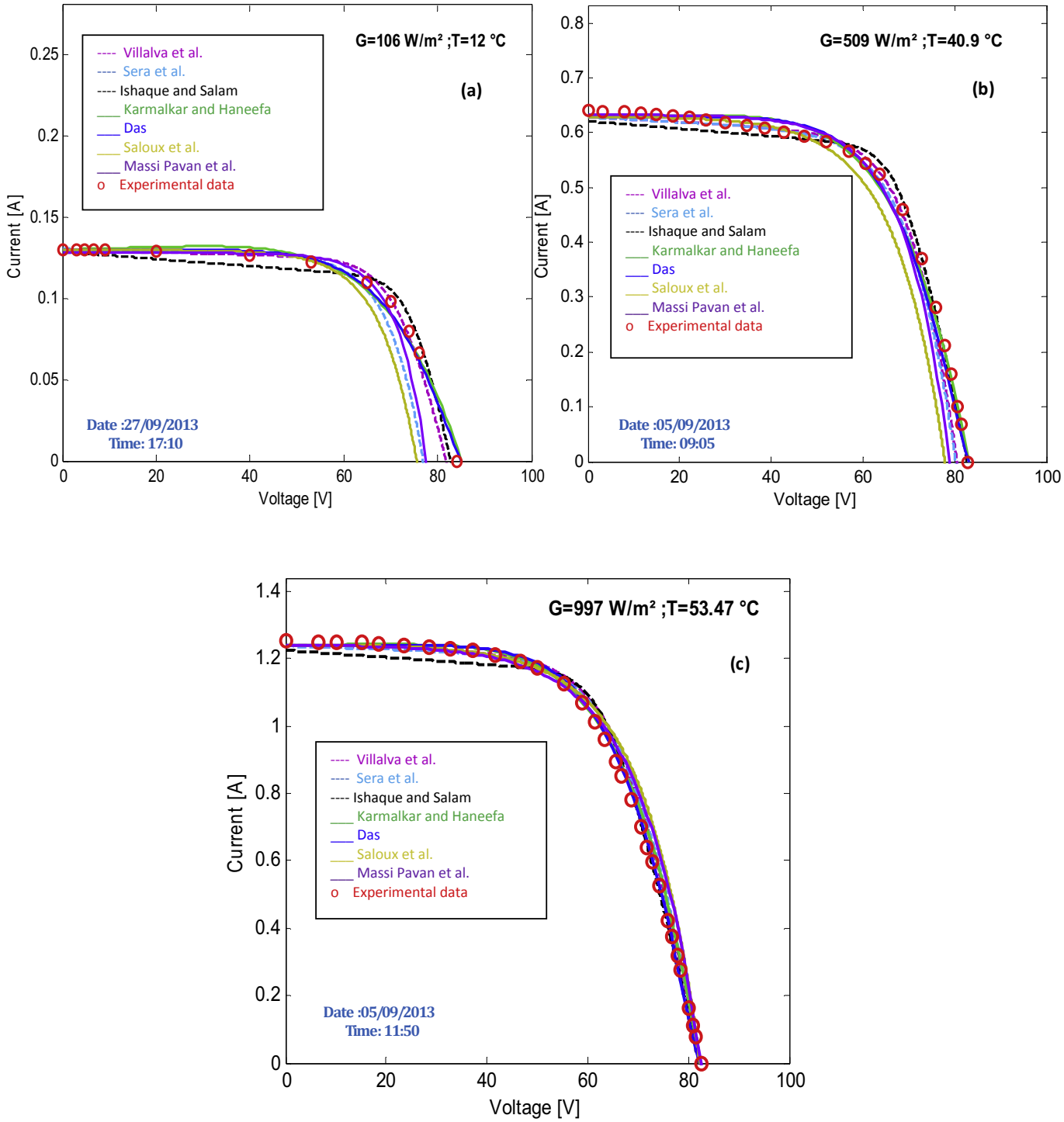

Fig. 15. Test 2:Measured vs simulated I-V characteristics of FS-272 at (a) low irradiance, (b) medium irradiance and (c) high irradiance.

4. Concluding remarks

This work presents a comparative study of seven models, published in the literature, for I-V prediction behaviour. The performances of these models have been assessed comparing their output both with data from manufacturers and from experimental measurements.

With reference to the obtained result, the following concluding remarks:

- With reference to the multi-crystalline silicon technology and with the exception of Saloux et al. all models predict the actual behaviour of the modules with a good degree of accuracy. The model by Massi Pavan et al. [13] has the highest accuracy in estimating the maximum power of the PV module at different operating conditions. However, at low irradiance, the models by Massi Pavan et al. [13] and by Saloux et al. [26] have low accuracy in the vicinity of the open circuit voltage;

Table 7a
Maximum Power and PRE_{Mpp} for Q.Pro 230 module (Test 2).

Operating conditions	Measured.P_{mp} (W)	Villalva et al.	Sera et al.	Ishaque and Salam	Karmalkar and Haneefa	Saloux et al.	Das	Massi Pavan et al.
M_{pp}(W)								
G = 135 W/m^2; T = 28 °C	27.5 ± 1.1	28.07	28.87	28.74	28.05	25.83	28.06	27.83
G = 479 W/m^2; T = 37 °C	101.2 ± 4.05	101.97	102.52	103.82	101.71	97.57	101.81	101.62
G = 906 W/m^2; T = 57 °C	155.34 ± 6.21	155.91	155.25	155.15	155.43	156.85	155.50	155.66
PRE_{Mpp}(%)								
G = 135 W/m^2; T = 28 °C		2.07 ± 0.08	4.98 ± 0.20	4.51 ± 0.18	2.00 ± 0.08	6.07 ± 0.24	2.03 ± 0.08	1.20 ± 0.05
G = 479 W/m^2; T = 37 °C		0.76 ± 0.03	1.30 ± 0.05	2.58 ± 0.10	0.50 ± 0.02	3.58 ± 0.14	0.68 ± 0.03	0.60 ± 0.02
G = 906 W/m^2; T = 57 °C		0.37 ± 0.02	0.06 ± 0.01	0.12 ± 0.01	0.06 ± 0.01	0.97 ± 0.04	0.10 ± 0.01	0.21 ± 0.01

Table 7b
Maximum power and RPE_{Mpp} for Q.Smart UF95module (Test 2).

Operating conditions	Measured. P_{mp} (W)	Villalva et al.	Sera et al.	Ishaque and Salam	Karmalkar and Haneefa	Saloux et al.	Das	Massi Pavan et al.
M_{pp}(W)								
G = 127 W/m^2; T = 11 °C	12.03 ± 0.48	11.85	11.25	11.75	11.91	10.29	11.88	11.93
G = 490 W/m^2; T = 21 °C	46.58 ± 1.86	46.11	45.60	46.08	46.26	43.90	46.23	46.32
G = 800 W/m^2; T = 35 °C	71.7 ± 2.87	72.22	71.94	73.12	71.88	71.03	71.91	71.53
PRE_{Mpp}(%)								
G = 127 W/m^2; T = 11 °C		1.49 ± 0.06	6.48 ± 0.26	2.33 ± 0.09	0.99 ± 0.04	14.46 ± 0.58	1.24 ± 0.05	0.83 ± 0.03
G = 490 W/m^2; T = 21 °C		1.00 ± 0.04	2.10 ± 0.08	1.07 ± 0.04	0.36 ± 0.01	5.75 ± 0.23	0.75 ± 0.03	0.56 ± 0.02
G = 800 W/m^2; T = 35 °C		0.72 ± 0.03	0.33 ± 0.01	1.98 ± 0.08	0.25 ± 0.01	0.93 ± 0.04	0.29 ± 0.01	0.24 ± 0.01

Table 7c
Maximum power and RPE_{Mpp} for FS-272 module (Test 2).

Operating conditions	Measured. P_{mp} (W)	Villalva et al.	Sera et al.	Ishaque and Salam	Karmalkar and Haneefa	Saloux et al.	Das	Massi Pavan et al.
M_{pp}(W)								
G = 106 W/m^2; T = 12 °C	7.15 ± 0.29	7.35	6.92	7.44	7.08	6.79	7.06	7.22
G = 509 W/m^2; T = 40.9 °C	32.64 ± 1.31	33.73	32.98	34.86	32.45	30.81	32.90	32.84
G = 997 W/m^2; T = 53.47 °C	62.80 ± 2.51	65.22	64.73	65.66	63.16	64.59	63.30	63.09
PRE_{Mpp}(%)								
G = 106 W/m^2; T = 12 °C		2.79 ± 0.11	3.22 ± 0.13	4.06 ± 0.16	0.98 ± 0.04	5.04 ± 0.2	1.54 ± 0.06	0.84 ± 0.03
G = 509 W/m^2; T = 40.9 °C		3.33 ± 0.13	1.04 ± 0.04	6.8 ± 0.27	0.58 ± 0.02	5.61 ± 0.22	0.80 ± 0.03	0.61 ± 0.02
G = 997 W/m^2; T = 53.47 °C		3.85 ± 0.15	3.07 ± 0.12	4.55 ± 0.18	0.57 ± 0.02	2.85 ± 0.11	0.79 ± 0.03	0.46 ± 0.02

- For thin-films CIGS and CdTe technologies, the use of explicit models is recommended. The models by Karmalkar and Haneefa [24] and Das [28] should be used for the best estimation of the I-V characteristics at different solar irradiances levels. Concerning the prediction of the maximum power point, the model by Massi Pavan et al. [13] provides excellent results. The model by Saloux et al. [26] should be used only at high irradiance, since at low irradiance it underestimates both power and open circuit voltage;
- The main drawbacks of implicit models (mainly based on numerical methods) are that they are sensitive to the initial values and often fail to converge. Moreover, they usually require complex iterative processes (Parameters identification by evolutionally algorithms such as Genetic Algorithms, Particle Swarm Optimization, Artificial Bee Colony, Flower Pollination Algorithm, etc.). Therefore, explicit analytical approximation expressions, when available, have a distinct advantage and are convenient in several practical applications;
- It is noteworthy that explicit models are useful for design engineers to quickly and easily determine the performance of any PV module without performing complexes numerical calculations.

Acknowledgements

The second author expresses a special acknowledgment to the International Centre for Theoretical Physics (ICTP), Trieste, Italy.

References

[1] IEA. A snapshot of global Markets. 2015.
[2] Green MA, Emery K, Hishikawa Y, Warta W, Dunlop ED. Solar cell efficiency tables (Version 48). Prog Photovolt. Res Appl 2016;24(7):903–13.
[3] Massi Pavan A, Mellit A, De Pieri D, Lughi V. A study on the mismatch effect due to the use of different photovoltaic modules classes in large-scale solar parks. Prog Photovolt. Res Appl 2014;22(3):332–45.
[4] Cañete C, Carretero J, Sidrach-de-Cardona M. Energy performance of different photovoltaic module technologies under outdoor conditions. Energy 2014;65:295–302.
[5] Ciulla G, Lo Brano V, Franzitta V, Trapanese M. Assessment of the operating temperature of crystalline PV modules based on real use conditions. Int J Photoenergy 2014:2014.
[6] Armstrong S, Hurley W. A thermal model for photovoltaic panels under varying atmospheric conditions. Appl Therm Eng 2010;30(11):1488–95.
[7] Pantic LS, Pavlovic TM, Milosavljevic DD, Radonjic IS, Radovic MK, Sazhko G. The assessment of different models to predict solar module temperature, output power and efficiency for Nis. Serbia Energy 2016;109:38–48.
[8] Torres-Ramírez M, Nofuentes G, Silva J, Silvestre S, Muñoz J. Study on analytical modelling approaches to the performance of thin film PV modules in sunny inland climates. Energy 2014;73:731–40.
[9] Josephs R. Solar cell array design handbook. NASA; 1976.
[10] Di Piazza M, Luna M, Petrone G, Spagnuolo G. About the identification of the single-diode model parameters of high-fill-factor photovoltaic modules. Conference about the identification of the single-diode model parameters of

high-fill-factor photovoltaic modules. IEEE, p. 85–91.
[11] Luque A, Hegedus S. Handbook of photovoltaic science and engineering. John Wiley & Sons; 2011.
[12] Veissid N, Bonnet D, Richter H. Experimental investigation of the double exponential model of a solar cell under illuminated conditions: considering the instrumental uncertainties in the current, voltage and temperature values. Solid-State Electron 1995;38(11):1937–43.
[13] Pavan AM, Mellit A, Lughi V. Explicit empirical model for general photovoltaic devices: experimental validation at maximum power point. Sol Energy 2014;101:105–16.
[14] Villalva MG, Gazoli JR. Comprehensive approach to modeling and simulation of photovoltaic arrays. Power Electron. IEEE Trans 2009;24(5):1198–208.
[15] Sera D, Teodorescu R, Rodriguez P. PV panel model based on datasheet values, Conference PV panel model based on datasheet values. IEEE, p. 2392–2396.
[16] De Soto W, Klein S, Beckman W. Improvement and validation of a model for photovoltaic array performance. Sol Energy 2006;80(1):78–88.
[17] Brano VL, Orioli A, Ciulla G, Di Gangi A. An improved five-parameter model for photovoltaic modules. Sol Energy Mater Sol Cells 2010;94(8):1358–70.
[18] Ishaque K, Salam Z, Taheri H. Simple, fast and accurate two-diode model for photovoltaic modules. Sol Energy Mater Sol Cells 2011;95(2):586–94.
[19] Khanna V, Das B, Bisht D, Singh P. A three diode model for industrial solar cells and estimation of solar cell parameters using PSO algorithm. Renew Energy 2015;78:105–13.
[20] Muhsen DH, Ghazali AB, Khatib T, Abed IA. Extraction of photovoltaic module model's parameters using an improved hybrid differential evolution/electromagnetism-like algorithm. Sol Energy 2015;119:286–97.
[21] AlHajri M, El-Naggar K, AlRashidi M, Al-Othman A. Optimal extraction of solar cell parameters using pattern search. Renew Energy 2012;44:238–45.
[22] Zagrouba M, Sellami A, Bouaïcha M, Ksouri M. Identification of PV solar cells and modules parameters using the genetic algorithms: application to maximum power extraction. Sol Energy 2010;84(5):860–6.
[23] Almonacid F, Rus C, Hontoria L, Muñoz F. Characterisation of PV CIS module by artificial neural networks. A comparative study with other methods. Renew Energy 2010;35(5):973–80.
[24] Karmalkar S, Haneefa S. A physically based explicit–model of a solar cell for simple design calculations. Electron Device Lett IEEE 2008;29(5):449–51.
[25] Das AK. Analytical expression of the physical parameters of an illuminated solar cell using explicit J–V model. Renew Energy 2013;52:95–8.
[26] Saloux E, Teyssedou A, Sorin M. Explicit model of photovoltaic panels to determine voltages and currents at the maximum power point. Sol Energy 2011;85(5):713–22.
[27] Saleem H, Karmalkar S. An analytical method to extract the physical parameters of a solar cell from four points on the illuminated curve. Electron Device Lett IEEE 2009;30(4):349–52.
[28] Das AK. An explicit J–V model of a solar cell for simple fill factor calculation. Sol Energy 2011;85(9):1906–9.
[29] Karmalkar S, Saleem H. The power law J–V model of an illuminated solar cell. Sol Energy Mater Sol Cells 2011;95(4):1076–84.
[30] Miceli R, Orioli A, Di Gangi A. A procedure to calculate the I–V characteristics of thin-film photovoltaic modules using an explicit rational form. Appl Energy 2015;155:613–28.
[31] Das AK, Karmalkar S. Analytical derivation of the closed-form power law–model of an illuminated solar cell from the physics based implicit model. Electron devices. IEEE Trans 2011;58(4):1176–81.
[32] Pavan A, Castellan S, Sulligoi G. An innovative photovoltaic field simulator for hardware-in-the-loop test of power conditioning units. Conference an innovative photovoltaic field simulator for hardware-in-the-loop test of power conditioning units.
[33] Massi Pavan A, Lughi V. Photovoltaics in Italy: toward grid parity in the residential electricity market. Conference Photovoltaics in Italy: toward grid parity in the residential electricity market. IEEE, p. 1–4.
[34] http://www.q-cells.com. Multi-crystalline Solar Module Q.Pro 225–240.
[35] http://www.q-cells.com. CIGS Solar module Q.Smart UF 75–95.
[36] http://www.firstsolar.com. Thin film CdTe technology First Solar FS-270-280.
[37] https://weatherspark.com/averages/32319/Trieste-Friuli-Venezia-Giulia-Italy.
[38] www.lsi-lastem.it. Data logger for environmental applications MW8024-02/10, Global radiation sensors pyranometers MW8008.1-05/11, Pt100 1/3 DIN – IEC 751.
[39] www.hobut.co.uk. Standard brass ended shunts.